Engineering Geology 314 (2023) 106998

Contents lists available at ScienceDirect

Engineering Geology

journal homepage: www.elsevier.com/locate/enggeo

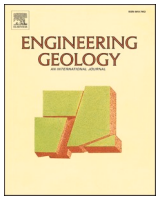

A Pareto–Poisson process model for intermittent debris flow surges developing from slope failures

Xiaojun Guo [a], Yong Li [a,*], Yingjie Yao [b], Daochuan Liu [c], Jun Zhang [a,d]

[a] Key Laboratory of Mountain Hazards and Surface Processes / Institute of Mountain Hazards and Environment, Chinese Academy of Sciences, Chengdu 610041, China
[b] Faculty of Science, The University of Hong Kong, Hong Kong, SAR, China
[c] Sichuan Highway Planning, Survey, Design and Research Institute Ltd., Chengdu 610041, China
[d] University of Chinese Academy of Sciences, Beijing 100049, China

ARTICLE INFO

Keywords:
Debris flow surge
Shallow slope failure
Poisson process
Pareto distribution
Random simulation

ABSTRACT

Many debris flows originate from shallow slope failures over the source area of valley and move in form of successive surges. In order to understand the behavior of such failures, we conducted seven sets of experiments of rainfall-induced soil failures in a 4 × 8 m spot on a slope under different rainfall intensities ranging from 12 to 60 mm/h, according to the local rainfall conditions in the valley of Jiangjia Gully, and this work is based on the experimental data. It is found that the failures are realization of a Poisson process with failure volume satisfying the Pareto distribution, thus the failure process can be simulated using a combinative Pareto-Poisson process (PPP) model. The PPP model incorporates a Poisson process determining the failure time, and a Pareto distribution characterizing the fluctuation of failure volume. The developing course of a debris flow surge is reduced to the hierarchic evolution of the failures from their source to the mainstream, which amounts to a cascade thinning process of the Poisson sequence in the PPP model framework. Given the controlling parameters (i.e., the Poisson intensity, Pareto distribution parameters, and thinning ratio), the model is capable of predicting surge sequences that agree well with the monitored surges in terms of time interval, magnitude fluctuation, and probability distribution. This study represents the first attempt to formulate a stochastic framework for debris flows developing from source to mainstream, which applies to debris flows fed by discontinuous material supplies from shallow slope failures.

1. Introduction

The phenomenon of surge waves is ubiquitous in debris flows throughout the world (Suwa et al., 1997; Berti et al., 1999; Rickenmann and Weber, 2000; Marchi et al., 2002). Such surges can originate owing to geomorphologic complexity (Coe et al., 2008; Theule et al., 2012; Kean et al., 2013), source distribution (Takahashi, 2014), grain size segregation (Gray and Ancey, 2009), and flow instability (Ng and Mei, 1994; Iverson and Denlinger, 2001; Arai et al., 2013). Because most surges occur in stream channels with gentle slope (~3°–10°), move slowly (<5.0 m/s), and have a low Froude number (F_r) (e.g., <2/3), their occurrence cannot be generally ascribed to flow instability, which has impact only under the conditions of steep slope and high F_r (e.g., ≥1) (Carasso and Shen, 1977; Zanuttigh and Lamberti, 2007).

Despite the various potential origins of material in debris flows, e.g., from mobilization of streambed sediment, transition of large landslides, or small slope failures, a common feature is that the material supply is random and discontinuous (Iverson et al., 1997; Hungr et al., 2014; Thouret et al., 2020; Guo et al., 2013, 2020). Many studies have investigated the source identification (e.g., Benda et al., 2003; Takahashi, 2014), soil–flow transition (Iverson et al., 1997, 2000; Wang and Sassa, 2001, 2003), substrate sediment initiation (Takahashi, 1978; Gregoretti, 2000; Gregoretti and Fontana, 2008), and dynamics of debris flows (e.g., Savage and Hutter, 1991; Iverson, and Denlinger., R. P., 2001; Blatz et al., 2004; Collins and Znidarcic, 2004; Iverson and George, 2014); however, an integrated scenario of debris flow development from source to the mainstream remains lacking.

Here, we propose a stochastic scenario of surge developing from discontinuous shallow slope failures based on our field experiments and observations conducted in Jiangjia Gully (JJG) (Guo et al., 2021), which is a well-known debris flow watershed in southwestern China. First, we identify the shallow slope failures as a spatial Poisson process with

* Corresponding author.
E-mail address: ylie@imde.ac.cn (Y. Li).

https://doi.org/10.1016/j.enggeo.2023.106998
Received 20 May 2022; Received in revised form 20 December 2022; Accepted 5 January 2023
Available online 18 January 2023

magnitude satisfying the Pareto distribution (i.e., the power law in general). Then, we formulate a combinative model incorporating the Poisson and Pareto elements to produce the failure sequence over the source area, and simulate surges by thinning the sequences from initial failure to the mainstream channel. The resultant surge sequence proves consistent with observational data. The developed model is the first in the study of debris flow that has capability of predicting the spatiotemporal characteristics (e.g., the magnitude fluctuation and the probability distribution) of surges, and the proposed scenario provides new insight into the formation and variation of debris flows originating from discrete shallow slope failures over a wide source area.

2. Spatiotemporal characteristics of debris flow surges in JJG

2.1. Background of JJG and debris flows

Debris flows in JJG are remarkable for their variety, and each debris flow event can contain tens or hundreds of surges distinct in material composition and flow regime, with peak discharge fluctuating in the range of 10–2500 m^3/s (Liu et al., 2009; Li et al., 2012; Guo et al., 2020; Zhang et al., 2021). Long-term observations carried out by the Dongchuan Debris Flow Observation and Research Station (DDFORS), Chinese Academy of Sciences, since the 1960s, have achieved a dataset of approximately 10,000 surges in 500 events (Cui et al., 2005; Guo et al., 2020). In recent years, Surges in JJG are typically viscous and originate from shallow failures of the colluvium slopes (< 5 m, about 30°– 40°) in the source area (e.g., Guo et al., 2013) (Fig. 1). In the preceding paper, we've reported the results of a group of experiments in a 4 × 8 m spot on a slope under different rainfall intensities ranging from 12 to 60 mm/h, according to the local rainfall conditions, which provided illustration of how the failures develop into intermittent surges (Guo et al., 2021); and the present work makes an attempt to formulate a quantitative framework accounting for the failure-developed debris flow, based on the spatiotemporal features of the failures.

2.2. Spatiotemporal features of surge sequences

Each debris flow event in JJG consists of a surge sequence. Despite the high variability of individual surges, the entire sequence appears to share several remarkable properties pertaining to the mechanism of surge formation.

1) Magnitude fluctuation

Surges cover a wide spectrum from hyperconcentrated flow to viscous flow, with varying velocity (0.1–15 m/s), discharge (10^0–10^3 m^3/s), and density (1.30–2.40 g/cm^3) (Fig. 2). The fluctuation differs remarkably from roll waves, where flow instabilities produce waves with increasing period and amplitude, and the first surge usually has the greatest depth and the longest duration (Zanuttigh and Lamberti, 2007).

2) Probability distribution

The discharge and velocity of a surge satisfy the family of exponential distributions, e.g., the exponential and Weibull distributions (Liu et al., 2008; Li et al., 2012), indicating that the majority of surges have discharge and velocity below the average. In particular, most surges have a low value of Froude number, F_r (e.g., <2/3), implying that they cannot have derived from instability, which usually occurs at higher values of F_r (Arai et al., 2013; Barker et al., 2017; Viroulet et al., 2018;

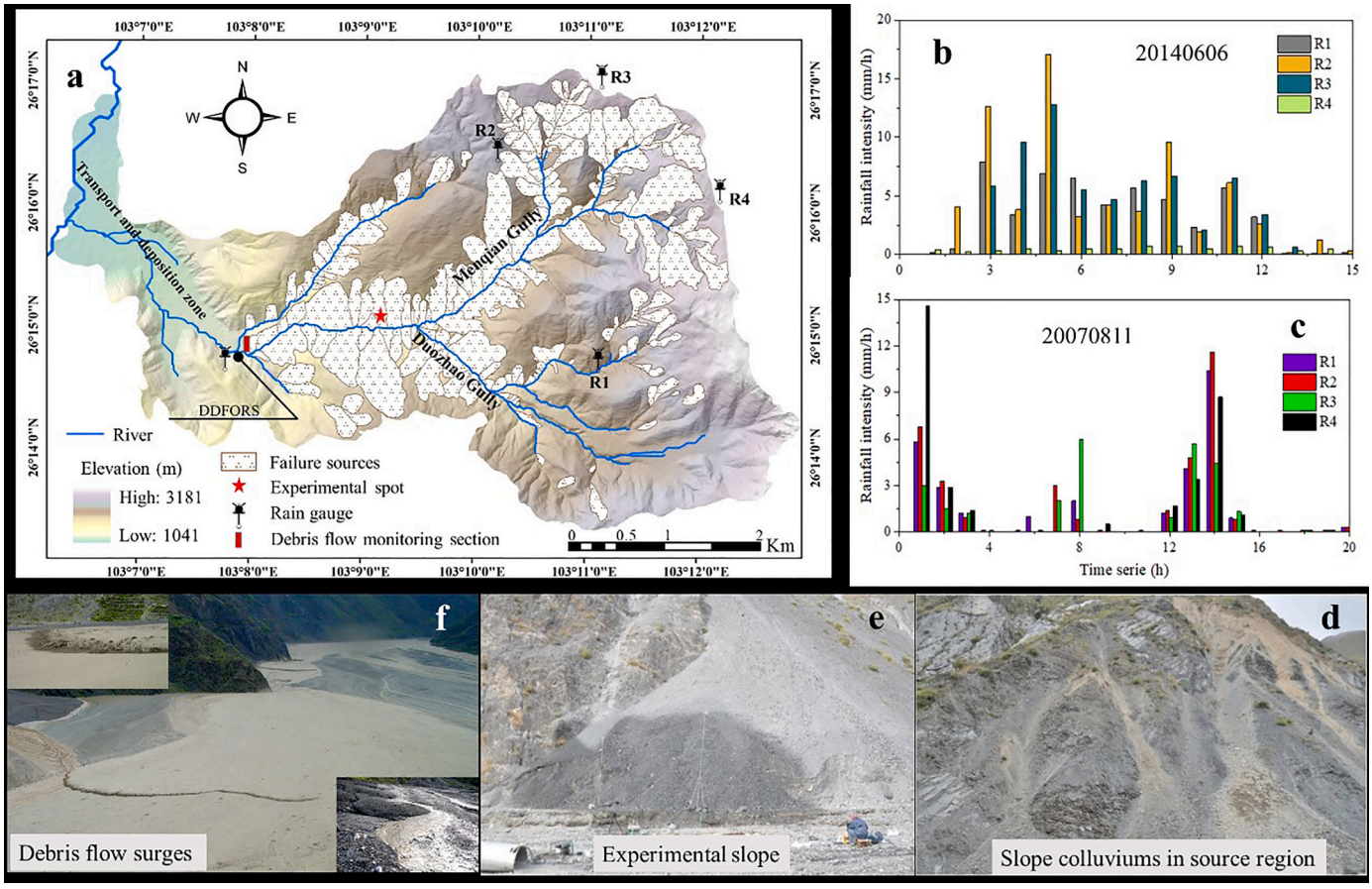

Fig. 1. Sources of debris flows in Jiangjia Gully (JJG): (a) the JJG watershed, (b) and (c) rainfall records at different gauges, (d) source slope, (e) experimental spot on a slope, and (f) successive surges in the mainstream channel. DDFORS: Dongchuan Debris Flow Observation and Research Station.

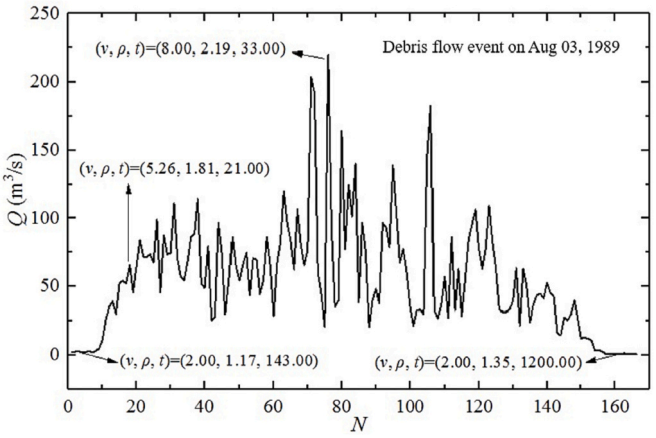

Fig. 2. Fluctuation of surges in a debris flow event, showing the high variability of flow density (ρ), velocity (v), discharge (Q), and time interval (t). N in horizontal axial is the surge sequence.

Razis et al., 2019).

3) Temporal intermittency

Surges are separated at time intervals of the order of approximately 100 s, following the exponential distribution. Observation indicates that the time interval decreases exponentially with flow density. This is understandable because high rainfall intensity causes high frequency (short intervals) and large number of failures, leading to rapid supply of mass that in turn results in surges of high density in short intervals. Thus, the temporal characteristics of surges are well associated with mass supply and present randomness in terms of sediment transport (e.g., Benda and Dunne, 1997).

In the following, we formulate a scenario to incorporate all the phenomena based on observations and field experiments.

3. Pareto–Poisson process of slope failures

3.1. Observation of field experiments on soil failures of source slopes

We conducted seven sets of experiments of rainfall-induced shallow soil failures in a 4 × 8 m spot on a slope in JJG under different rainfall

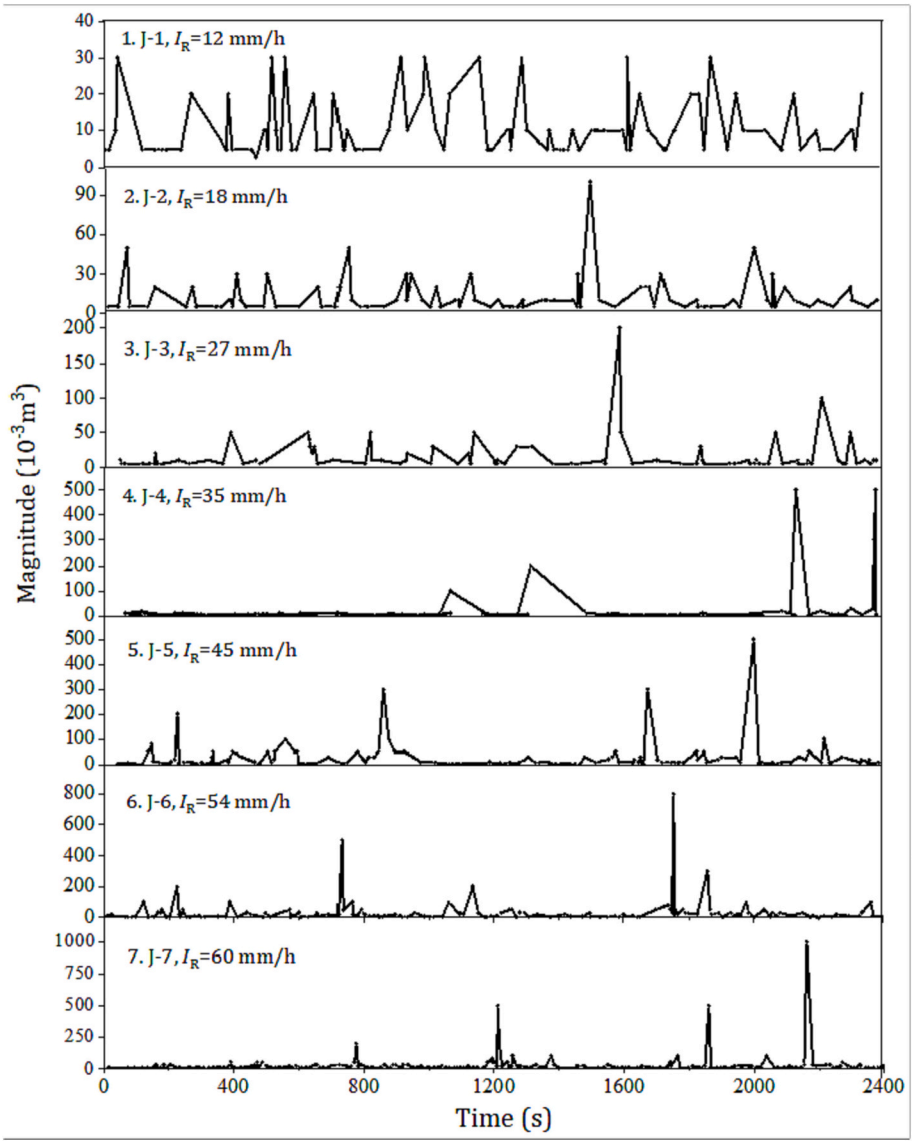

Fig. 3. Failure sequences on the test spot of a slope in JJG under different rainfall intensities.

intensities, I_R, which was set as 12, 18, 27, 36, 45, 54, and 60 mm/h, according to the local rainfall conditions (Guo et al., 2013). Here "failure" is used as a general term including various shallow soil movements and their detached soil bodies (e.g., Varnes, 1978; Hungr et al., 2014). The rainfall duration and running time of each experiment was 40 min, after which the failures stopped and the slope resumed a state of repose. The failure time, location and volume are recorded in a coordinate of cell grids of the slope, by both directly reading snapshots and combining field observation. The experiments display a sequence of slope failures and the subsequent flows formed by the failures into the channel. The resultant failure sequences are shown in Fig. 3, and the parameters and quantities considered are summarized in Table 1 (for details of the experiments, see Guo et al. (2021).

3.2. Statistical features of the failure sequences

The failure sequences exhibit several fundamental statistical features.

1) Power law distribution of failure volume (magnitude)

Failure volume (M; unit: 10^{-3} m^3) fluctuates by up to three orders of magnitude, i.e., in the range of ~5–800 10^{-3} m^3, and presents a power law distribution (Guo et al., 2021):

$$P(\rangle M) = P(M,\beta) = K_M M^{-\beta} \quad (1)$$

where $P(>M)$ is the fraction of failures greater than M. K_M is the coefficient, and β is the exponent. The power law occurs universally in catastrophic events, especially landslides over large areas (e.g., Guzzetti et al., 2002; Marchi and D'Agostino, 2004; Malamud et al., 2004; Hungr et al., 2008; Jakob and Friele, 2010). The occurrence of the power law here implies that the failures represent an intrinsically random process.

2) Exponential distribution of time interval

The time interval between failures is in the range of 10–180 s (on average of 20 s), and presents an exponential distribution (Guo et al., 2021):

$$P(\rangle T) = C_T\, exp(-\lambda T), \quad (2)$$

where $P(>T)$ is the time interval longer than T. C_T is the coefficient, and λ is the exponent. The parameters of Eqs. 1 and 2 are listed in Table 2.

3) Parameters in relation to rainfall intensity

The parameters above are related to the rainfall intensity governing the experiments:

$$X = C_X\, exp.(k_X I_R) \quad (3)$$

where the subscript X denotes the involved parameters, i.e., representing coefficients in relationship of failure number (N), time interval (T), interval distribution (λ), failure volume (M), and volume distribution (β). C_X and k_X are the coefficient the exponent, respectively (Table 3).

Eq. (4) provides a wealth of information concerning the effects of rainfall intensity on such slope failure. As rainfall intensity (I_R) rises, the failure number (N_c), frequency ($1/T_m$ or λ), mean volume (M_c), and total quantity (M_t) all increase exponentially (Guo et al., 2021). Thus, Eq. 4 provides an estimate of the mass supplied by such failures:

$$M_t = N_c M_c = C_N C_M exp((k_{M+}\, k_N) I_R) \sim exp(0.044 I_R), \quad (4)$$

which is well confirmed by experiment. Therefore, rainfall intensity imposes a nonlinear effect on the mass supplied to debris flows.

High rainfall intensity causes a high concentration of mass supply, leading to high-density surges with short intervals, as mentioned above. Thus, a failure sequence provides quantitative hints regarding the surges, and finding the link between them was the object of this study.

Table 1
Summary of soil failures on the source slope under different rainfall conditions.

No.	I_R	N_C	T_0	T_m	T_{max}	M_{max}	M_T	M_c
J-1	12	93	–	25.54	111	30	998	11.47
J-2	18	92	–	25.83	95	100	1173	12.61
J-3	27	87	35min08s	27.14	129	200	1395	15.16
J-4	36	97	17min51s	24.47	175	500	2305	23.76
J-5	45	141	10min16s	16.8	61	500	3846	27.28
J-6	54	152	10min04s	15.79	51	800	5001	32.9
J-7	60	222	7min36s	10.27	58	1000	5928	26.7

Note: I_R: rainfall intensity (mm/h); N_C: failure number; T_0: occurrence of first failure; T_m: mean interval (s); T_{max}: longest interval (s); M_{max}: maximal failure size (10^{-3} m^3); M_c: mean failure size (10^{-3} m^3); M_T: total failure size (10^{-3} m^3).

Table 2
Parameters of the distributions for failure magnitude and time interval.

Experiments	I_R (mm/h)	K_M	β	T (s)	λ
J-1	12	8.22	1.2657	25.54	0.0391
J-2	18	8.80	1.2590	25.83	0.0387
J-3	25	8.08	1.1940	27.14	0.0368
J-4	36	7.23	1.0580	24.47	0.0409
J-5	45	8.05	1.0620	16.8	0.0595
J-6	54	7.59	1.0191	15.79	0.0633
J-7	60	6.50	1.0470	10.27	0.0970

3.3. Identifying the stochastic process of slope failure

3.3.1. Statistical test of the failure sequences

The failure sequences (Fig. 3) can be expressed as time series in terms of failure volume:

$$\{S_0\} = \{M_{T(i)} \,|\, i = 0, 1, 2, \ldots..N\}, \quad (5)$$

where $M_{T(i)}$ is the failure occurring at time $T(i)$, and N is the number of failures; and the time interval $\Delta T_i = T_i - T_{i-1}$ satisfies the exponential distribution.

To recognize the nature of the sequence, we must first check the stationarity and randomness. The Mann–Kendall test (Hamed and Rao, 1998) indicates that the sequences have no significant trend, and the nonparametric run test (i.e., the Wald–Wolfowitz test) (Alhakim and Hooper, 2008) finds they are random at the 95% confidence level. Therefore, the sequence can be considered random and stationary, and the exponential distribution can be further established by passing traditional tests such as the χ^2 and Kolmogorov goodness-of-fit tests (Clauset et al., 2007), which confirm the goodness-of-fit at the 0.05 significance level. Then, the exponential distribution of the time interval, as a sufficient and necessary condition, indicates that the failure sequence results from a Poisson process (Lari et al., 2014; Krishnan, 2015).

The Poisson process is the simplest and most random way of describing certain events in the sense that a process is almost inevitably a Poisson process only if the individual events are independent (e.g., Kingman, 1992; Straub and Schubert, 2008). Failures scattered on a slope can be considered statistically independent in both space and time. Equivalent to the exponential distribution of the time interval, the probability of n failures occurring within interval t follows the Poisson distribution:

$$\text{Prob}\{N(t) = n\} = p_n(\lambda t) = \frac{(\lambda t)^n}{n!} e^{-\lambda t}, \quad (6)$$

The parameter λ is the reciprocal of the expected interval T_m (Table 1); hence, it reflects the average number of events occurring within unit time. In this sense, λ represents the intensity of the process.

The failure number is $N = \lambda T$, with T being the duration. Because λ is

Table 3
Exponents for failure interval and size varying with rainfall intensity.

Parameters	T_{int}		N_c		M_c		λ		β	
	C_T	k_T	C_N	k_N	C_M	k_M	C_λ	k_λ	C_β	k_β
Values	45.1	−0.022	53.3	0.021	8.94	0.022	0.22	0.021	1.33	−0.005

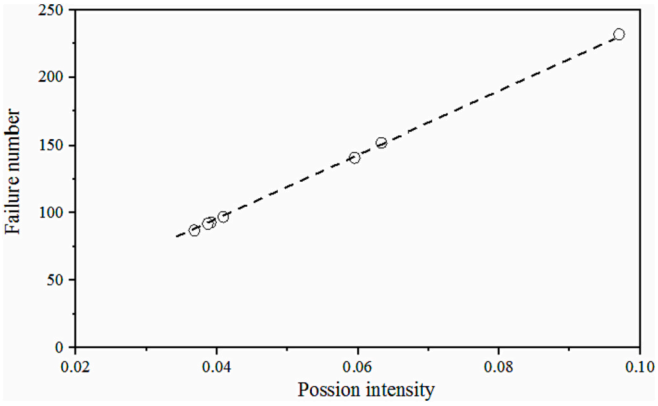

Fig. 4. Linear *N–T* relationship providing convincing evidence for identifying the Poisson process.

derived from the time interval and is statistically independent of the failure number, the linear *N–T* relationship (Fig. 4) provides convincing evidence of the Poisson process.

3.3.2. Slope failure as a Pareto–Poisson process (PPP)

The distributions of the time interval and failure volume (Eqs. 1 and 2) determine a failure sequence. As the power law is not really a probability density function, a truncated form obtained through normalization is often used instead (e.g., Newman, 2005):

$$p(x) = \frac{\alpha - 1}{m_0}\left(\frac{x}{m_0}\right)^{-\alpha}, \tag{7}$$

which is the Pareto distribution that describes the statistics of observed data surpassing a certain threshold value (Embrechts et al., 1997). Here, m_0 is the scale parameter defining the threshold, and α is the shape parameter describing the "long tail" of the distribution. Therefore, the failure sequence can be expressed as follows:

$$\{S_0\} = \left\{M_{T(i)} \,|T(i) = \text{Poisson}(\lambda)\,; M_i = \text{Power}(\alpha m_0)\right\}, \tag{8}$$

This means that the Poisson parameter determines when a failure occurs, and that the Pareto parameter determines how the volume varies. The parameters relevant to our experiments are listed in Table 4.

The Pareto exponent α is also related to rainfall intensity:

$$\alpha = C_P exp(-k_P I_R), \tag{9}$$

where $C_P = 2.21$ and $k_P = 0.004$ ($R^2 = 0.80$).

The value of m_0 falls into two groups: ~5.05 for low I_R and 5.21 for high I_R, which makes a considerable difference between failures under low and high rainfall intensity. It should be noted that the median failure volume ($m_{1/2}$), which divides the distribution into two equal halves, is.

$$M_{1/2} = 2^{1/(\alpha-1)} m_0, \tag{10}$$

Then, the fraction of larger failures (i.e., at the right-hand half) is.

$$R = \left(m_{1/2}/m_0\right)^{-\alpha+2} = 2^{-(\alpha-2)/(\alpha-1)}, \tag{11}$$

which causes different outcomes for $\alpha > 2$ and $\alpha < 2$. For $\alpha > 2$, the majority of failure quantity is concentrated on the minority of large failures; for $\alpha < 2$, R is not well defined and almost all the failure quantity is derived from large failures. Because $\alpha > 2$ occurs at low I_R, we have mean failure volume $< m \geq m_0(\alpha - 1)/(\alpha - 2)$; however, for high I_R and $\alpha < 2$, the distribution has no finite mean value because the maximal failure increases indefinitely with the number of failures (Newman, 2005). Therefore, the Pareto exponent distinguishes the effects of low and high rainfall intensity. Considerable fluctuation in failure volume is expected to occur at high I_R.

The failure sequence (Eq.8) is determined by:

$$\{S_0(I_R)\} = \left\{M_{T(i)} \,|T(i) = \text{Poisson}\left(e^{k_\lambda I_\lambda}\right); M_i = \text{Pareto}\left(m_0 e^{-k_\lambda I_\lambda}\right)\right\}, \tag{12}$$

Thus, the failure might be rightly called a PPP with parameters depending only on rainfall intensity. Because all the parameters are obtained from field experiments, this provides a physically based picture of slope failure. Fig. 5 presents a simulated failure sequence at $I_R = 54$ mm/h for comparison with the experimental results, highlighting the agreement in volume fluctuation and temporal interval.

3.4. Surges from slope failures

Parts of the failures will turn into separate surges when they move downward in the stream channel (Guo et al., 2021). A surge at time t_j, $S_1(j)$, is formed by the failures that occur between t_j and t_{j+1} through a random process:

$$S_1(j) = \sum_{t_j < t < t_{j+1}} \zeta(t) S_0(t), (j = 0, 1, 2, \ldots.), \tag{13}$$

where $\{S_0\}$ represents the failures and $\{S_1\}$ represents the surges that result directly from the failures. The map $\{S_0\} \rightarrow \{S_1\}$ describes the first transition step from failures to surges in the tributary channel under the influence of slope.

The coefficient $\zeta(t)$ takes the role of "selecting" failures that provide material supply to a surge. For individual failures, $\zeta(t)$ depends on soil-water interaction, whereas for the entire failure sequence, $\zeta(t)$ is in effect a random variable. Our experiments indicate that small failures are inclined to "attach" the streambed or mix with water as a hyperconcentrated flow. Only failures exceeding a certain threshold would turn into debris flows. For example, at $I_R = 54$ mm/h, the threshold is $M_c \approx 50$ (10^{-3} m^3), meaning that only 16% of failures are effective as suppliers to surges, accounting for 67% of the mass. It is a simple step to determine the effective mass fraction from the Pareto distribution.

Table 4
Parameters determining failure sequence in the experiments.

Parameters	J1	J2	J3	J4	J5	J6	J7
I_R(mm/h)	12	18	25	36	45	54	60
α	2.14	2.06	2.03	1.82	1.75	1.71	1.83
m_0	5.02	5.08	5.04	5.08	5.25	5.23	5.14
λ_0	0.0391	0.0387	0.0368	0.0409	0.0595	0.0633	0.097

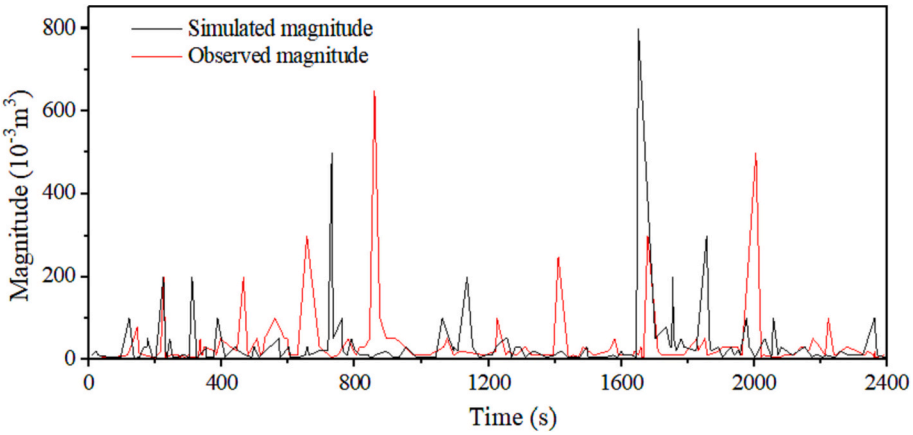

Fig. 5. Simulated failure sequence at $I_R = 54$ mm/h, in comparing with the observed sequence.

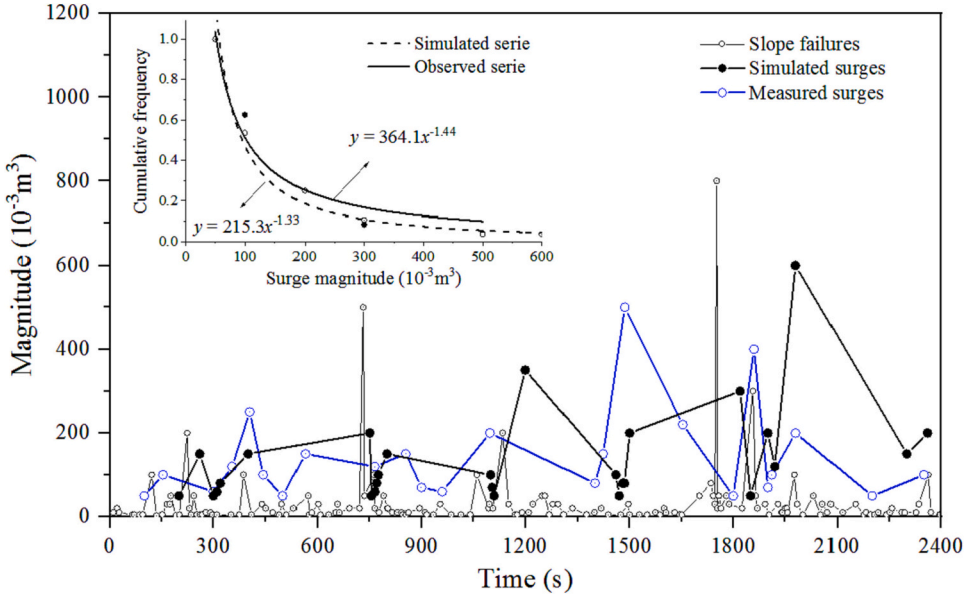

Fig. 6. Observed and simulated surge sequence from failures ($I_R = 54$ mm/h), with the cumulative frequency distribution of surge volume shown in the inset.

Fig. 6 shows the simulation at $I_R = 54$ mm/h in comparison with the observed surges. The real process contains 24 surges with mean soil volume of 141 (in unit of 10^{-3} m^3/s, similarly hereinafter) and total volume of 3400, while the simulation yields 28 surges with average volume of 138, and total volume of 3880. Moreover, the simulated surge sequence presents the same power law distribution of magnitude (inset in Fig. 6). From this example, it can be seen that the PPP model has the capability of predicting the intermittent surges from the failures. In the following, we apply this scenario to the watershed.

It is noted that, the soil failures occurring in a sequence are only determined by the rainfall intensity; while the length of the sequence, or the number of failures, is controlled by the duration time of rainfall. In other words, a long-duration rainfall may lengthen the process and increase the number of failures, but the duration time as a quantity does not necessarily determine the duration of the event.

4. Surges developing on the watershed scale

4.1. Conceptual framework of hierarchic development from failures to surges

The discussion above illustrates how tributary surges develop from failures. In reality, these tributary surges might continue moving downstream, enter streams of ever-increasing order of magnitude, and finally converge into surges in the mainstream. To achieve such a picture requires complete knowledge of surges in tributaries and their developing routes, which is beyond any campaign of field observations or laboratory experiments. Here, we take an overall viewpoint, ignore details of intermediate processes, and simplify the surge evolution as a cascading process from source to mainstream in the hierarchic system of the watershed (Fig. 7).

In this framework, the failures occur randomly in all possible sources, and the surge develops as the following cascading process:

$$\{S_0\}\rightarrow\{S_1\}\rightarrow\{S_2\}\rightarrow\ldots\rightarrow\{S_j\}\ldots\rightarrow\{S_f\}, \tag{14}$$

where $\{S_0\}$ represents the failure sequence, $\{S_i\}$ represents the intermediate mass sequences, and $\{S_f\}$ represents the final sequence as the mainstream surges. Thus, this tributary process (or the first step of soil-flow transition, Eq.13) occurs repeatedly in streams of various order of magnitude throughout the watershed.

4.2. Controlling parameters of surge development

The cascading process (Eq.14) is governed by the Poisson intensity λ,

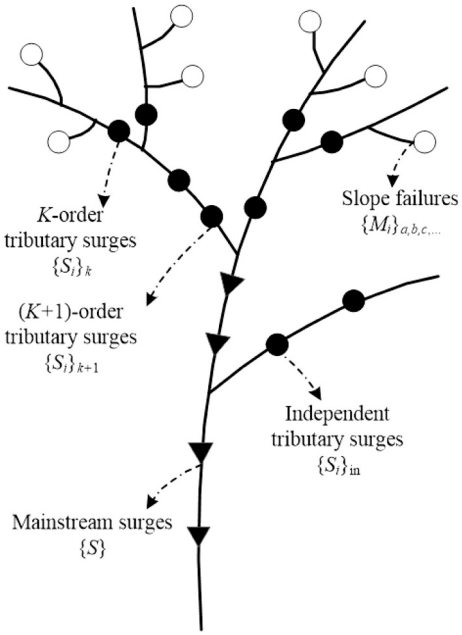

Fig. 7. Conceptual framework of surge development from source areas to mainstream channel in a self-similar hierarchic watershed valley system.

the Pareto parameter α, and the effective coefficient ζ of soil-flow transition, which can be determined as described below.

1) Poisson intensity of failures over the sources

The Poisson intensity λ is determined by the local rainfall intensity. Over the watershed, the failures represent the sum of numerous Poisson processes on different slopes. Following the additivity of the Poisson process, which claims that independent Poisson variables $X_j = P(\lambda_j)$ have a sum that retains the Poisson property: $\Sigma X_i = P(\Sigma\lambda_j)$, the failures over the entire source area will have the following intensity:

$$\lambda_0(R) = \sum_{R_i}(A_i/A_E) \Big/ \lambda_{Ei}\,, \tag{15}$$

where subscript "0" means the sources (0-order tributary) in the hierarchic system of the watershed, λ_E is the intensity at I_R, A_E is the area of the test spot (i.e., 32 m^2 in our experiments), and A_i is the area of the i-th source with the same soil condition (for the present, we do not consider soil heterogeneity over the sources, which matters little for the generality of the scenario). Here, the test λ_E is determined by the empirical correlation $\lambda_E = C_\lambda \exp(k_\lambda I_R)$ (Eq.3 and Table 3), and the sources can be identified through the rainfall distribution. We have several gauges in the source areas (Fig. 1), each of which records the rainfall covering an effective source area. Therefore, the potential sources can be identified by field survey and spatial interpretation of rainfall. Table 5 lists the controlling parameters for the given rainfall events (in the table, "-" means no rainfall recorded at the gauge.)

This over-source intensity λ_0 has an intuitive explanation, i.e., the failure is a Bernoulli event satisfying a binomial distribution, with each event occurring with small probability p; however, over all the sources, the number n would become large such that $np = \lambda_0$ determines the collective activities of failure. Table 5 lists the local rainfall intensity at each gauge (c.f. Fig. 1) and the corresponding overall λ_0 (with the Pareto exponent α) for several debris flow events in JJG.

Table 5
Controlling parameters of the PPP simulation based on rainfall distribution.

Events	I_{R1}	I_{R2}	I_{R3}	I_{R4}	λ_0	α
E080705	–	19.3	19.4	18.8	195.5	2.00
E990818	6.4	12.7	–	19.5	774	2.06
E990716	47	2.4	–	24.7	555	2.63
E000704	32	21.6	–	37.8	245.4	1.57
E080701	–	37.9	25.6	37.9	178.5	1.86
E030605	32.5	22.3	–	57.8	189.9	1.65

2) Effective coefficient of soil-flow transition

The cascading transition (Eq. 14) follows the mass-transition rule:

$$S_{I+1}(j) = \sum_{T_{j-1}<t_i<T_j} \zeta(Ii) S_I(t_i), \tag{16}$$

where the capital subscript I denotes the order of the sequence. This describes a sequence of thinning Poisson processes (e.g., Resnick, 2007), which means that each element in the sequence takes a contributing probability represented by $\zeta(i)$. The j-th element in the thinned sequence is supplied by elements between T_{j-1} and T_j in the preceding sequence. Moreover, the thinned sequence retains the nature of the Poisson process but takes a new intensity, $\lambda(S_{I+1}) = \rho\lambda(S_I)$, with the time interval increasing by $1/\rho$. For a single slope, $\zeta(I, i)$ is random and acts as an "effective coefficient" of mass supply.

4.3. Realization of the processes from failures to mainstream surges

1) Failures over the sources

Taking event E990818 (i.e., the debris flow occurrence on Aug 18, 1999; the same code applies to other events, e.g., in the following Table 8) as an example, and using the parameters in Table 5 ($\lambda_0 = 774.0$, $\alpha = 2.06$, and given $m_0 = 5.0$ for low I_R), we are able to generate the initial failures $\{S_0\}$ over the sources (Eq.12), setting a 6-h duration on the basis of the recorded rainfall. This causes 16,718,400 failures (Fig. 8a), amounting to a total volume of 52,761 m^3.

2) Cascading transition from soil to flow

Field observations and experiments in JJG indicate that approximately one third of the failure mass contributes to tributary surges. The total sediment of E990818 is 13,305 (m^3), i.e., ~30% of the simulated quantity. Therefore, one third is considered a proper ratio of the effective supply from the failures. Considering the self-similarity of the processes in the watershed, we assume the coefficient ζ in Eq.16 is constant, which gives the following transition rule:

$$M_f = \zeta^n M_0, \tag{17}$$

where n is the number of cascading steps.

3) Thinning of the sequence

As the sequence develops, the time interval increases. In the source areas, the failures occur at short intervals (e.g., $1/\lambda_0 \approx 1/774 = 0.0012$ s) as if they were continuous over a large area. However, in a local spot, they are separated by an obvious interval (of the order of 10s), as observed in the experiments. Up to the mainstream sequence $\{S_f\}$, the time interval is elongated to the order of 100 s owing to the thinning of the Poisson process. For this, we have a "thinning probability," or a ratio, of intensity: $\lambda_{i+1} = \rho\lambda_i$, ($i = 0, 1, 2, \ldots, f$), meaning that:

$$T_f = (1/\rho^n\lambda_0) = \rho^{-n} T_0, \tag{18}$$

Field observations in the last tributaries (i.e., those joining the mainstream) indicate that the interval between surges is of the order of 10s, which implies $\rho \approx 0.10$. From 10^{-3} s in the source area to 10^2 s in the mainstream, Eq.18 gives $n = 5$. This is a very specific and sensitive value. If $n = 6$, T_f would rise to 1000s, far beyond the real values. This

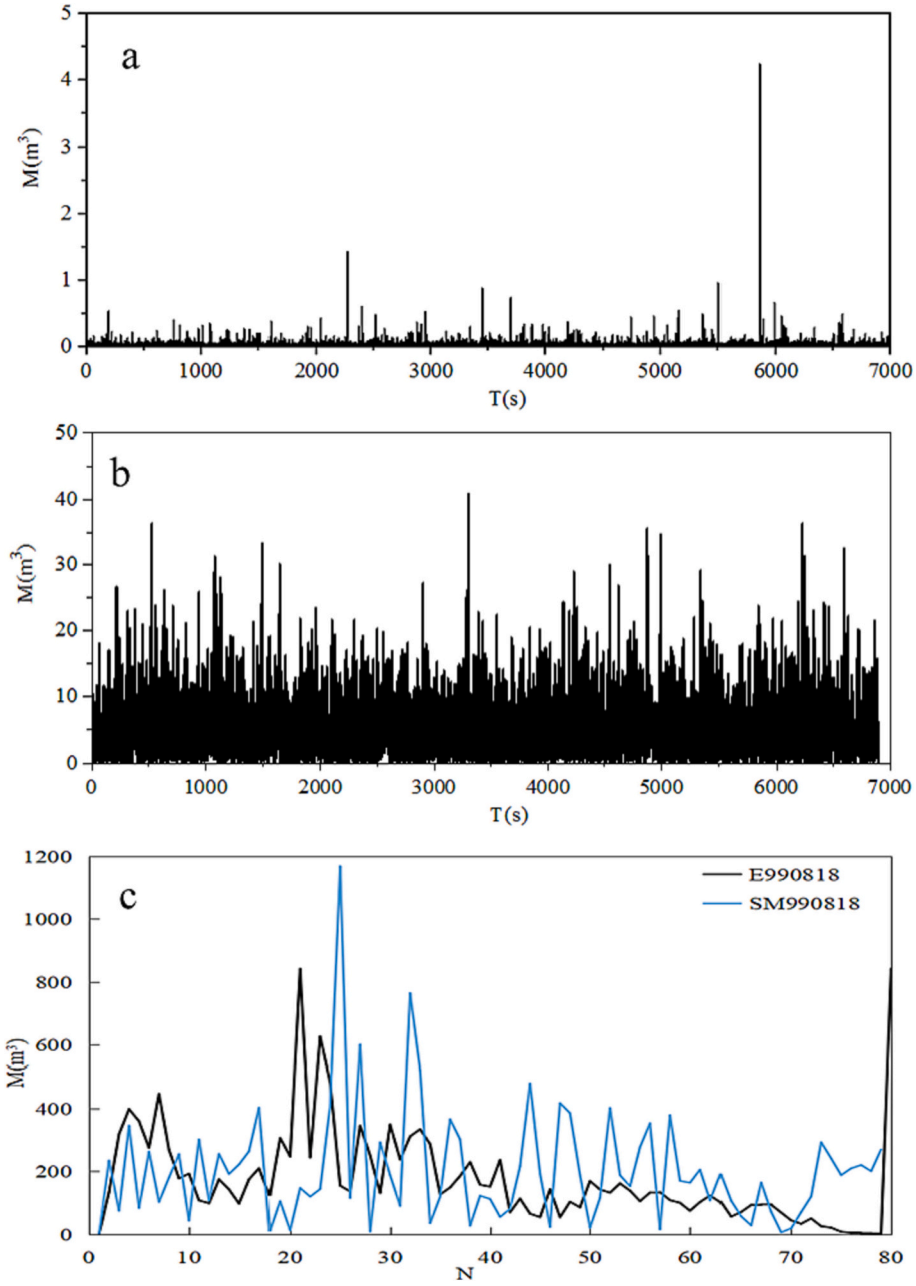

Fig. 8. Cascading process of mass developing from source failures to mainstream surges. (a) Initial failure sequence $\{S_0\}$ over the source areas, (b) mass sequence in the third order $\{S_3\}$, and (c) the ultimate sequence representing the mainstream surges.

agrees well with the fact that debris flows never develop in streams of higher order. For E990818, the time interval is 84 s on average, and Eq.18 gives $\rho \approx 0.11$; thus, $\zeta = 0.79$, which means that at each transition step, the mass loss is approximately 21%.

4) Sequence development from source to mainstream

Given the initial sequence $\{S_0\}$ generated by the controlling parameters (Fig. 8a), we can calculate the high-order $\{S_i\}$ through the thinning operation. For instance, the interval of $\{S_1\}$ is $\lambda_1 = \rho\lambda_0 = 77.4$, which yields a sequence of time intervals $\{T_1, T_2, \ldots, T_N\}$. Then, the mass at T_i is contributed by the failures in $\{S_0\}$ within $(T_{i\text{-}1}, T_i)$, with $\zeta = 0.79$. Repeating the operation leads to the final sequence.

The coefficient ζ gives a lower limit for the mass supply and can be determined through the Pareto distribution of failure volume. The Pareto parameter α determines a threshold M_c, where failures below which do not contribute to the next step of development. Owing to the so-called 80/20 law (i.e., the large failures of only 20% account for 80% of the total) (e.g., Lipovctsky, 2009), the contributing failures might still account for a large quantity.

Table 6 lists the parameters of each step of the thinning process, in which N is the element number of the sequence at each step, M_T is the

Table 6
Parameters for cascade thinning of the mass transition sequences.

	N	λ	M_T (m^3)	$<T>_s$ (s)
$\{S_0\}$	5,340,430	744.00	52,761	0.0013
$\{S_1\}$	574,236	81.57	41,099	0.012
$\{S_2\}$	60,383	8.94	34,797	0.11
$\{S_3\}$	6598	0.98	28,446	1.05
$\{S_4\}$	692	0.11	20,899	9.97
$\{S_f\}$	78	0.012	16,146	88.40

total mass volume, and $< T >_s$ is the average time interval. At the final step $\{S_f\}$, the time interval is comparable with that between observed surges (i.e., 84 s), and M_T represents the total volume of observed sediment delivery (1, 3305 m^3).

Fig. 8 shows three steps of the development sequence. The final sequence (Fig. 8c) is expected to represent the surge sequence in the mainstream, with which we plot the observed mainstream surges (only sediment being counted here) for comparison. It is noted that the fluctuation decreases greatly in the thinned sequences. In the following, we see that the thinning process cuts the "long tail" of the Pareto distribution and reduces the power law to an exponential function.

Similarly, the PPP model may apply to general cases. Table 7 lists several debris flow events in JJG, and Fig. 9 displays the basic quantities of simulated and observed surges, in which N is the observed number of surge, M_s is the total sediment volume (m^3), M_0 is the simulated total supplies of failure supplies (m^3); and other terms are the same as those in Table 1-3. The simulation reproduces the fluctuation pattern of surges. In particular, the simulated M_{max} agrees well with reality, which is directly derived from the thinning of the failure sequence governed by λ_0 and ρ. This means that the simulation has the capability of predicting the surge sequence and the fundamental statistical features.

4.4. Generalizing the simulation parameters

In the above, we verified the PPP model through simulations using target events to estimate the transition ratio ρ. However, an applicable model should make predictions using parameters that can be predetermined through operable routines. For this, we consider how the parameters vary between events. It should be noted that the three events under consideration (E990818, E010708, and E080701) represent three categories (c.f. Tables 5 and 7), i.e., in different situations of rainfall intensity, surge number, and magnitude. The ratio ρ varies in the range of 0.10–0.15, and this can be taken as representative of the general case. Moreover, ρ appears to decrease with λ_0 in a power law form, i.e., $\rho \approx \lambda_0^{-m}$ ($m \approx 0.15$, e.g., Fig. 10), which means ρ decreases exponentially with I_R because λ_0 increases exponentially with local rainfall intensity (i.e., $\lambda_E \approx \exp.(k_\lambda I_R)$). This leads to a short interval of the surge sequence, which agrees with the observations.

In short, it is possible to determine the parameters from the rainfall distribution, and the key point is to identify the sources responding to the rainfall distribution. This is similar to the case of hydrologic simulation, where one has provable and applicable models but yet parameters need to be determined empirically. In this respect, it would be a long way to go for generally determining model parameters in practice.

4.5. Verifying simulations through statistical properties of surge sequences

4.5.1. Temporal variation of surge sequences

For a random event, the reliability of a simulation relies on the statistical properties, e.g., the temporal variation and probability distribution. We can define a time-dependent average (or the moving average) of mass, as follows:

$$\langle M \rangle_n = \sum_1^n M_i \,, \tag{19}$$

The simulations reproduced the variation patterns of the surge sequences, which are comparable with the observations, as shown in Fig. 11 (with "S" denoting the simulated result). Roughly speaking, the fluctuation patterns fall into three categories:

(a) surges that fluctuate in the first episode and then decay in a gentle slope (E990818, E000704, and E080701, with $\lambda_0 = 774$, 245.4, and 178.5, respectively) (Fig. 11a);

(b) surges that increase persistently in the first half of the period and then decay slowly (E030605, with $\lambda_0 = 189.9$) (Fig. 11b);

(c) surges that fluctuate gently throughout the entire process (E080705 and E990716, with $\lambda_0 = 195.5$ and 552, respectively) (Fig. 11c).

Broadly, $<M>_n$ rises and then falls linearly: $<M>_n \approx \mathrm{sgn}(n - n_c) Kn$, where $\mathrm{sgn}(x)$ is the sign function. Here, the key point is the time (or surge number n_c) at which the curve approaches the peak. This is obviously governed by the details of the development processes (e.g., soil-water interactions in the tributaries and local conditions of the streambeds) and does not depend on an overall parameter (e.g., λ_0). Nevertheless, the moving average reveals the gross decay of the event and implies that most events transport sediment in the earlier stage of the course (e.g., Liu et al., 2008, 2009).

4.5.2. Scaling distribution of surge sediment

It is particularly interesting that the surge sediment satisfies a general scaling distribution:

$$P(M) = Cm^{-\mu} exp(-M/M_c), \tag{20}$$

where $P(M)$ is the exceedance percentage of surges with mass greater than M, C is the normalized coefficient, μ is an exponent, and M_c is a characteristic magnitude. It is found that $\mu = a\mathrm{Ln}C + b$, where a and b are constants, and the distribution is characterized by the two parameters μ and M_c. Table 8 lists the parameters of the test events, with goodness-of-fit of $R^2 \approx 1$. Furthermore, the distribution falls upon a single exponential curve $P^*(M) = \exp.(-M^*)$ when the coordinates are rescaled by $M^* = M/M_c$ and $P^*(M) = P(M)\, M^{\mu}/C$ (Fig. 12). The coinciding distribution curve implies the existence of a universal mechanism underlying the development of surge sequences from various sources, which qualifies the reasonability of the presented PPP model.

5. Discussion

The PPP model is conceptually simple and practically useful in predicting surge sequences. However, several problems concerning model application, verification, and limitation are worthy of further discussion.

5.1. Limitation and application

The PPP model proposed here is for intermittent debris flow surges originating from slope failures based on the in situ experiments simulating the rainfall-induced shallow soil failures and the following process of supplying the debris flows, and it does not pretend to encompass flows derived from transition of landslides (Iverson et al., 1997; Gabet and Mudd, 2006), failure of streambed sediment (Gregoretti and Fontana, 2008), or mobilization of deposits by the firehose effect (Coe et al.,

Table 7
Parameters and basic quantities of simulated sequences compared with observed events.

Events	Observations				Parameters		Simulation		
	T_m	N	M_s	M_{max}	λ_0	ρ	M_0	M_f	M_{max}
E080705	183	58	5.56	0.27	195.5	0.1228	17.43	5.1	0.38
E990818	85	78	13.31	0.84	774.0	0.1088	52.76	16.15	1.17
E990716	112	116	20.46	0.84	552.0	0.1101	67.27	20.86	0.87
E000704	113	71	7.49	0.32	245.4	0.1293	17.69	6.26	0.44
E080701	79	32	1.3	0.14	178.5	0.1479	4.92	1.85	0.21
E030605	158	40	5.33	0.52	189.9	0.1272	15.28	5.82	0.71

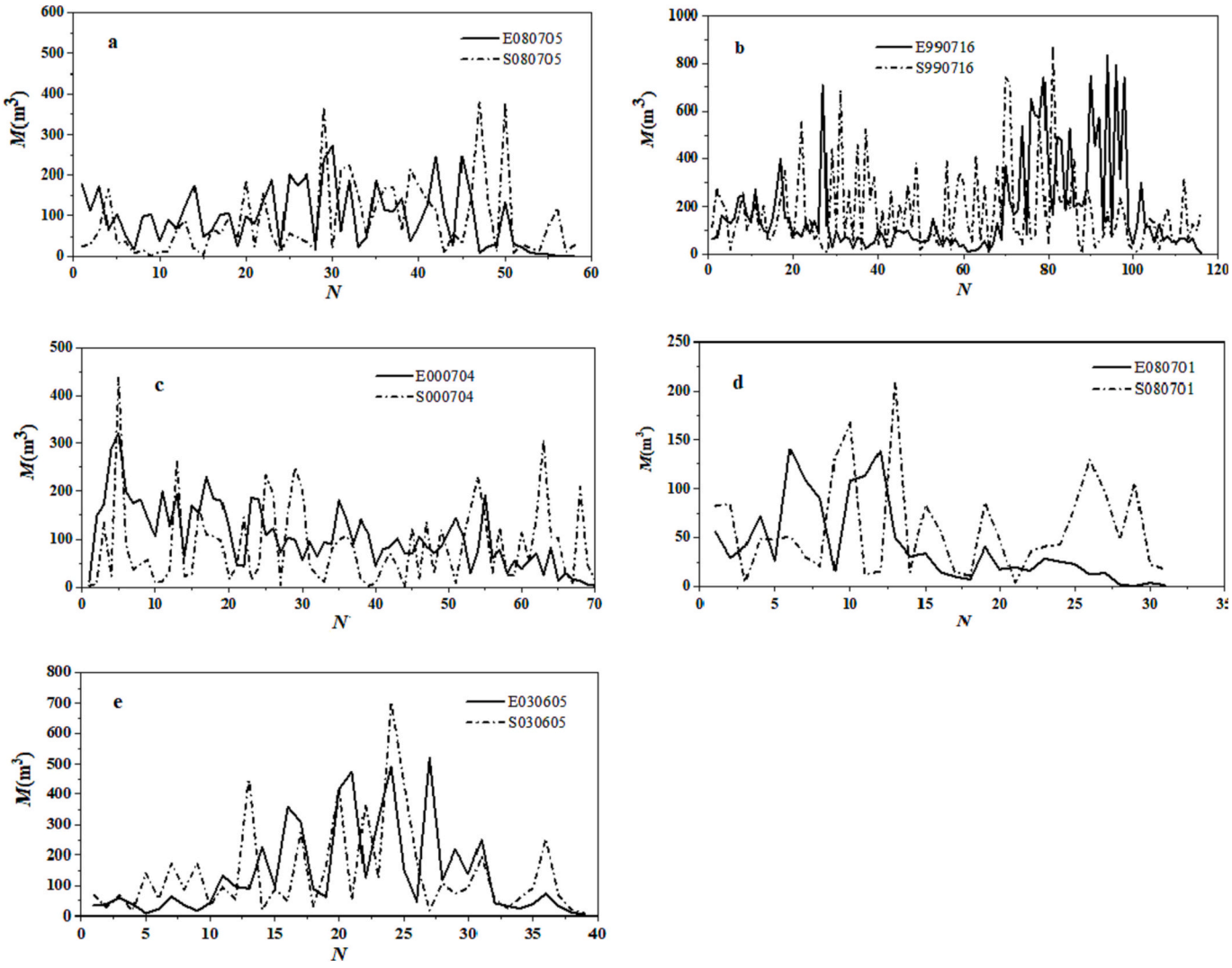

Fig. 9. Simulated surge sequences under different rainfalls compared with observed events.

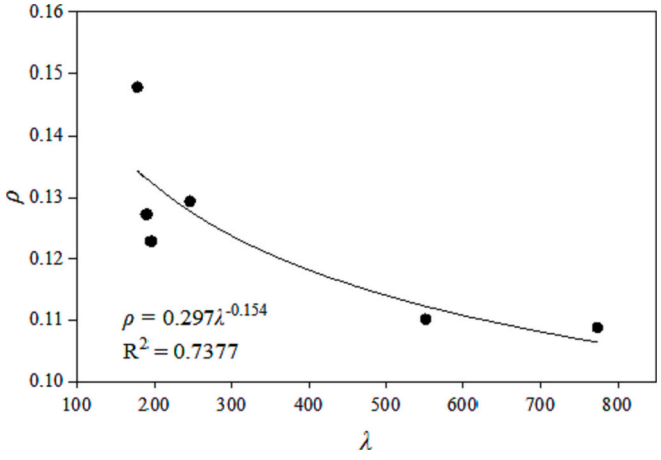

Fig. 10. The thinning factor decreases with Poisson intensity in a power-law form.

2008), which also might result in surges, as we observed in tributaries in JJG. In addition, the quantitative results of this work are based on the experiments on a single small slope, which inevitably leads to some limitations when applying to a watershed covering large area of source slopes.

Although we provide a plausible extrapolation from the spot experiments to the whole source areas, there are uncertainties in determining the involved parameters. Then, as a potentially practical framework for predicting intermittent debris flow surges from slope failures, the PPP model at present form is mainly conceptual. But for some special cases where the rainfall and material sources can be well identified, it may provide convincing predictions of the surge probability.

In addition, in the PPP model, the soils are assumed to be "active" owing to gravity rather than "passive" and stimulated by flushing water; therefore, the model considers only the processes of soil supply and ignores the hydrologic process. In fact, the hydrologic process sets the background of the soil processes, which facilitates the formation and development of debris flows, and should be considered in the future work.

5.2. *Sensitivity, reliability, and predictability*

The model depends on several empirical parameters: λ_0 determining the Poisson process of failure, α determining the Pareto distribution of failure volume, and ρ determining the effective mass supply to the surge. All these parameters are principally determined by rainfall intensity (e.g., Table 5), and thus the model can predict events under given rainfall conditions. However, the sensitivity to rainfall intensity means it is

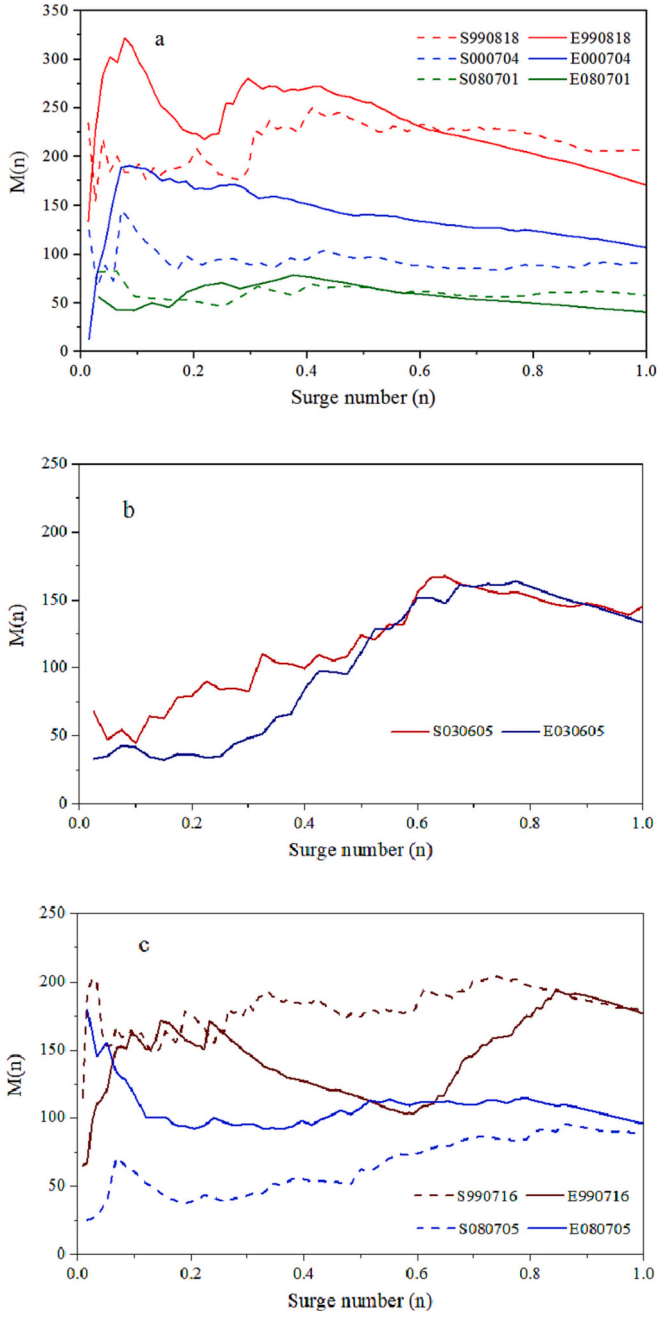

Fig. 11. Fluctuation of the moving average sediment volume of the surge sequence for different events (S and E represent the simulated and monitored debris flow surge sequences, respectively).

crucial to determine the rainfall distribution and to identify the responding sources, which is of great difficulty in practice because of the lack of accurate rainfall records at the slope scale (usually below 1 km^2), and the high spatial variability of rainfall in mountainous watersheds.

Nevertheless, it is possible for the PPP model to make a reasonable prediction of debris flows in the sense of susceptibility assessment, because the sources (determining λ_0) can be identified and localized to high accuracy through geographic information system interpretation and field survey (e.g., photos acquired by an unmanned aerial vehicle), and both α and ρ vary gently within certain ranges and can be considered as constant in specific situation. More importantly, the sensitivity to rainfall intensity and distribution reveals the drawback of the assessment based on the so-called rainfall threshold overall a watershed.

Table 8
Distribution parameters for surge sediment of simulated and real events.

Event		C	μ	M_c (m^3)
E080705	Real	0.9514	- 0.0785	144.5
	Sim	0.9329	- 0.0545	184.9
E990818	Real	0.8843	- 0.0965	217.5
	Sim	0.7135	- 0.1458	252.7
E990716	Real	1.045	- 0.0036	436.4
	Sim	0.8355	- 0.0873	286.8
E000704	Real	0.6156	- 0.2586	85.06
	Sim	0.966	- 0.0524	167.1
E080701	Real	1.014	- 0.0372	90.83
	Sim	0.9032	- 0.1016	89.88
E030605	Real	0.9708	- 0.0277	344.7
	Sim	0.952	- 0.0346	333.1

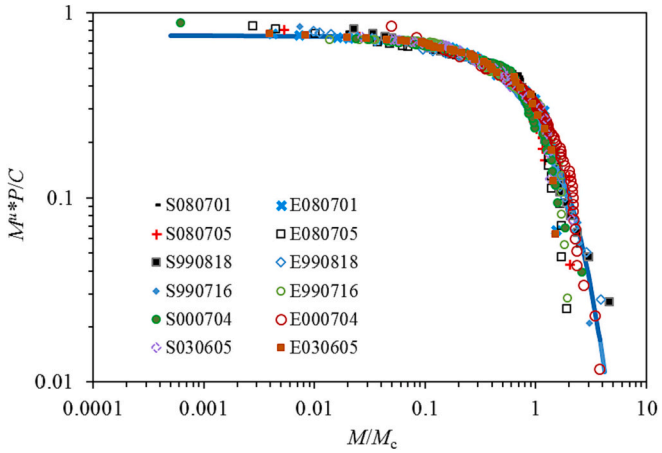

Fig. 12. Distribution of surge sediment of real and simulated surges.

5.3. Generalization and implications

Furthermore, for theoretical implications, the PPP model has revealed universal features of the cascading processes in a watershed, which might apply to a variety of hydrogeophysical processes. Actually, the model predicts a scaling distribution for the surges, which is spontaneously derived from the thinning of the power law distribution of the failures. This provides a mechanism for transition from the family of power law distributions to exponential distributions, as generally observed in relation to natural phenomena. The randomness of the mass supply and debris flow formation is universal in nature, which implies that one must evaluate a debris flow in relation to local conditions rather than the global environment of the watershed.

6. Conclusions

We proposed a stochastic scenario and a PPP model for intermittent surges based on experiments on a natural slope. This marks an attempt to establish a framework for debris flow development from source to the mainstream channel within a watershed, especially for the surge phenomenon in JJG, where debris flows usually originate from rainfall-induced shallow slope failures over a wide range of sources rather than from a specific large landslide. The model incorporates the Poisson process of slope failure and the Pareto distribution of failure volume, with controlling parameters determined by the rainfall distribution and intensity. Specifically, we derived the following conclusions.

1) The rainfall-induced slope failures can be considered as a Poisson process, for which the intensity parameter is determined by the rainfall intensity in the source areas. This determines the frequency or number of the failures.

2) The failure volume satisfies the two-parameter Pareto

distribution, with a nearly constant shape parameter and a scale parameter varying exponentially with rainfall intensity. This describes the magnitude fluctuation of the failures.

3) The shallow slope failures over the watershed may develop intermittent debris flow surges in the mainstream, which can be simulated by cascade thinning of the failure sequences. In this sense the surges are derived from a sequence of PPP processes.

4) The PPP model may produce different fluctuation patterns of surge discharge and derive a scaling distribution of surge sediment. The PPP scenario of debris flow also represents the cascading evolution of mass movements in the self-similar hierarchic system of a watershed.

Credit author statement

Xiaojun Guo: Conceptualization, Methodology, Data curation, Writing – original draft, Writing – review & editing. **Yong Li:** Conceptualization, Writing – review & editing, Funding acquisition. **Yingjie Yao:** Software, Investigation. **Daochuan Liu:** Investigation. **Jun Zhang:** Investigation.

Declaration of Competing Interest

None.

Data availability

Data will be made available on request.

Acknowledgments

This study is supported by the Strategic Priority Research Program of the Chinese Academy of Sciences (No. XDA23090202), the Second Scientific Expedition on the Qinghai-Tibet Plateau (2019QZKK0903-02), NSFC (41977257), the Key Science and Technology Projects of Transportation Industry (No. 2021-MS4-104) and Sichuan Provincial Transportation Science and Technology Project (No. 2021-A-08), and the Science and Technology Projects (2022JDJQ0008). We thank James Buxton, MSc, from Liwen Bianji (Edanz) (www.liwenbianji.cn), for editing the English text of a draft of this manuscript.

References

Alhakim, A., Hooper, W., 2008. A non-parametric test for several independent samples. J. Nonparametric Stat. 20 (3), 253–261. https://doi.org/10.1080/10485250801976741.

Arai, M., Huebl, J., Kaitna, R., 2013. Occurrence conditions of roll waves for three grain–fluid models and comparison with results from experiments and field observation. Geophys. J. Int. 195, 1464–1480. https://doi.org/10.1093/gji/ggt352.

Barker, B., Johnson, M.A., Noble, P., Rodrigues, L.M., Zumbrun, K., 2017. Note on the stability of viscous roll waves. Comptes Rendus Mécanique 345 (2), 125–129. https://doi.org/10.1016/j.crme.2016.11.001.

Benda, L., Dunne, T., 1997. Stochastic forcing of sediment supply to channel networks from landsliding and debris flows. Water Resour. Res. 33, 2849–2863. https://doi.org/10.1029/97WR02388.

Benda, L., Veldhuisen, C., Black, J., 2003. Debris flows as agents of morphological heterogeneity at low-order confluences, Olympic Mountains, Washington. Geol. Soc. Am. Bull. 115 (9), 1110–1121. https://doi.org/10.1130/B25265.1.

Berti, M., Genevois, R., Simoni, A., Tecca, P.R., 1999. Field observations of a debris flow event in the Dolomites. Geomorphology 29, 265–274. https://doi.org/10.1016/S0169-555X(99)00018-5.

Blatz, J.A., Ferreira, N.J., Graham, J., 2004. Effects of near-surface environmental conditions on instability of an unsaturated soil slope. Can. Geotech. J. 41 (6), 1111–1126. https://doi.org/10.1139/t04-058.

Carasso, A., Shen, M.C., 1977. On viscous fluid flow down an inclined plane and the development of roll waves. SIAM J. Appl. Math. 33 (3), 399–426. https://doi.org/10.1137/0133026.

Clauset, A., Shailizi, C.R., Newman, M.E.J., 2007. Power-law distributions in empirical data. SIAM Rev. 51 (4), 661–703. https://doi.org/10.1137/070710111.

Coe, J.A., Kinner, D.A., Godt, J.W., 2008. Initiation conditions for debris flows generated by runoff at Chalk Cliffs, Central Colorado. Geomorphology 96 (3–4), 270–297. https://doi.org/10.1016/j.geomorph.2007.03.017.

Collins, B.D., Znidarcic, D., 2004. Stability analyses of rainfall induced landslides. J. Geotech. Geoenviron. Eng. 130 (4), 362–372. https://doi.org/10.1061/(ASCE)1090-0241(2004)130:4(362).

Cui, P., Chen, X.Q., Wang, Y.Y., et al., 2005. Jiangia Ravine debris flows in South-Western China. In: Jakob, M., Hungr, O. (Eds.), Debris-Flow Hazards and Related Phenomena. Springer, Heidelberg, pp. 565–594.

Embrechts, P., Klüppelberg, C., Mikosch, T., 1997. Modelling extremal events- for Insurance and Finance. Springer Science & Business Media, 183–199 pp.

Gabet, E.J., Mudd, S.M., 2006. The mobilization of debris flows from shallow landslide. Geomorphology 74, 207–218. https://doi.org/10.1016/j.geomorph.2005.08.013.

Gray, J., Ancey, C., 2009. Segregation, recirculation and deposition of coarse particles near two-dimensional avalanche fronts. J. Fluid Mech. 629, 387–423. https://doi.org/10.1017/S0022112009006466.

Gregoretti, C., 2000. The initiation of debris flow at high slopes: experimental results. J. Hydraul. Res. 38 (2), 83–88. https://doi.org/10.1080/00221680009498343.

Gregoretti, C., Fontana, G.D., 2008. The triggering of debris flow due to channel-bed failure in some alpine headwater basins of the Dolomites: analyses of critical runoff. Hydrol. Process. An Int. J. 22 (13), 2248–2263. https://doi.org/10.1002/hyp.6821.

Guo, X.J., Cui, P., Li, Y., 2013. Debris flow warning threshold based on antecedent rainfall: a case study in Jiangjia Ravine, Yunnan, China. J. Mt. Sci. 10 (2), 305–314. https://doi.org/10.1007/s11629-013-2521-z.

Guo, X.J., Li, Y., Cui, P., Yan, H., Zhuang, J.Q., 2020. Intermittent viscous debris flow formation in Jiangjia Gully from the perspectives of hydrological processes and material supply. J. Hydrol. 589, 125–184. https://doi.org/10.1016/j.jhydrol.2020.125184.

Guo, X.J., Li, Y., Cui, P., Yan, Y., Wang, B.L., Zhang, J., 2021. Spatiotemporal characteristics of discontinuous soil failures on debris flow source slopes. Eng. Geol. 295, 106438 https://doi.org/10.1016/j.enggeo.2021.106438.

Guzzetti, F., Malamud, B.D., Turcotte, D.L., Reichenbach, P., 2002. Power-law correlations of landslide areas in Central Italy. Earth Planet. Sci. Lett. 195, 169–183. https://doi.org/10.1016/S0012-821X(01)00589-1.

Hamed, K.H., Rao, A.R., 1998. A modified Mann-Kendall trend test for autocorrelated data. J. Hydrol. 204, 182–196. https://doi.org/10.1016/S0022-1694(97)00125-X.

Hungr, O., McDougall, S., Wise, M., Cullen, M., 2008. Magnitude–frequency relationships of debris flows and debris avalanches in relation to slope relief. Geomorphology 96 (3–4), 355–365. https://doi.org/10.1016/j.geomorph.2007.03.020.

Hungr, O., Leroueil, S., Picarelli, L., 2014. The Varnes classification of landslide types, anupdate. Landslides 11, 167–194. https://doi.org/10.1007/s10346-013-0436-y.

Iverson, R.M., Denlinger., R. P., 2001. Flow of variably fluidized granular masses across three-dimensional terrain: 1. Coulomb mixture theory. J. Geophys. Res. Solid Earth 106 (B1), 537–552. https://doi.org/10.1029/2000JB900329.

Iverson, R.M., George, D.L., 2014. A depth-averaged debris-flow model that includes the effects of evolving dilatancy. I. Physical basis. Proc. Royal Soc. A Math. Phys. Eng. Sci. 470 (2170), 20130819. https://doi.org/10.1098/rspa.2013.0819.

Iverson, R.M., Reid, M.E., LaHusen, R.G., 1997. Debris-flow mobilization from landslides. Annu. Rev. Earth Planet. Sci. 25 (1), 85–138. https://doi.org/10.1146/annurev.earth.25.1.85.

Iverson, R.M., Reid, M.E., Iverson, N.R., LaHusen, R.G., Logan, M., Mann, J.E., Brien, D. L., 2000. Acute sensitivity of landslide rates to initial soil porosity. Science 290, 513–516. https://doi.org/10.1126/science.290.5491.513.

Jakob, M., Friele, P., 2010. Frequency and magnitude of debris flows on Cheekye River, British Columbia. Geomorphology 114 (3), 382–395. https://doi.org/10.1016/j.geomorph.2009.08.013.

Kean, J.W., McCoy, S.W., Tucker, G.E., Staley, D.M., Coe, J.A., 2013. Runoff-generated debris flows: Observations and modeling of surge initiation, magnitude, and frequency. J. Geophys. Res. Earth Surf. 118 (4), 2190–2207. https://doi.org/10.1002/jgrf.20148.

Kingman, J.F.C., 1992. Poisson Processes. Clarendon Press, 1992.

Krishnan, V., 2015. Probability and Random Processes, 2015. John Wiley & Sons.

Lari, S., Frattini, P., Crosta, G.B., 2014. A probabilistic approach for landslide hazard analysis. Eng. Geol. 182, 3–14. https://doi.org/10.1016/j.enggeo.2014.07.015.

Li, Y., Liu, J.J., Hu, K.H., Su, P.C., 2012. Probability distribution of measured debris-flow velocity in Jiangjia Gully, Yunnan Province, China. Nat. Hazards 60 (2), 689–701. https://doi.org/10.1007/s11069-011-0033-0.

Lipovctsky, S., 2009. Pareto 80/20 law: derivation via random partitioning. Int. J. Math. Educ. Sci. Technol. 40 (2), 271–277. https://doi.org/10.1080/00207390802213609.

Liu, J.J., Li, Y., Su, P.C., Cheng, Z.L., 2008. Magnitude–frequency relations in debris flow. Environ. Geol. 55, 1345–1354. https://doi.org/10.1007/s00254-007-1083-1.

Liu, J.J., Li, Y., Su, P.C., Cheng, Z.L., Cui, P., 2009. Temporal variation of intermittent surges of debris flow. J. Hydrol. 365, 322–328. https://doi.org/10.1016/j.jhydrol.2008.12.005.

Malamud, B.D., Turcotte, D.L., Guzzetti, F., Reichenbach, P., 2004. Landslide inventories and their statistical properties. Earth Surf. Process. Landf. 29 (6), 687–711. https://doi.org/10.1002/esp.1064.

Marchi, L., D'Agostino, V., 2004. Estimation of debris-flow magnitude in the eastern Italian Alps. Earth Surf. Process. Landf. 29, 207–220. https://doi.org/10.1002/esp.1027.

Marchi, L., Arattano, M., Deganutti, A.M., 2002. Ten years ofdebris-flow monitoring in the Moscardo torrent Italian Alps. Geomorphology 46 (1–2), 1–17. https://doi.org/10.1016/S0169-555X(01)00162-3.

Newman, M.E.J., 2005. Power laws, Pareto distributions and Zipf`s law. Contemp. Phys. 46 (5), 323–351. https://doi.org/10.1080/00107510500052444.

Ng, C.O., Mei, C.C., 1994. Roll waves on a shallow layer of mud modelled as a power-law fluid. J. Fluid Mech. 263, 151–183. https://doi.org/10.1017/S0022112094004064.

Razis, D., Kanellopoulos, G., van der Weele, K., 2019. A dynamical systems view of granular flow: from monoclinal flood waves to roll waves. J. Fluid Mech. 869, 143–181. https://doi.org/10.1017/jfm.2019.168.

Resnick, S.I., 2007. Heavy-Tail Phenomena: Probabilistic and Statistical Modeling. Springer Science & Business Media, New York pp.404.

Rickenmann, D., Weber, D., 2000. Flow resistance of natural and experimental debris-flows in torrent channels. In: Debris-flow Hazards Mitigation: Mechanics, Prediction and Assessment, pp. 245–254.

Savage, S.B., Hutter, K., 1991. The dynamics of avalanches of granular materials from initiation to runout. Part I: Analysis. Acta Mech. 86, 201–223. https://doi.org/10.1007/BF01175958.

Straub, D., Schubert, M., 2008. Modeling and managing uncertainties in rock-fall hazards. Georisk 2 (1), 1–15. https://doi.org/10.1080/17499510701835696.

Suwa, H., Sawada, T., Mizuyama, T., Arai, M., Takahashi, T., 1997. Observational Study on Viscous Debris Flows and Countermeasures against them. Proc. Intern. Symp. On Natural Disaster Prediction and Mitigation, Kyoto, pp. 401–406.

Takahashi, T., 1978. Mechanical characteristics of debris flow. J. Hydraul. Div. 104, 1153–1169. https://doi.org/10.1061/JYCEAJ.0005046.

Takahashi, T., 2014. Debris Flow: Mechanics, Prediction, and Countermeasures. CRCPress_Balkema.

Theule, J.I., Liebault, F., Loye, D., Laigle, D., Jaboyedoff, M., 2012. Sediment budget monitoring of debris-flow and bedload transport in the Manival Torrent, SE France. Nat. Hazards Earth Syst. Sci. 12 (3), 731–749. https://doi.org/10.5194/nhess-12-731-2012.

Thouret, J.C., Antoine, S., Magill, C., Ollier, C., 2020. Lahars and debris flows: Characteristics and impacts. Earth Sci. Rev. 201, 103003 https://doi.org/10.1016/j.earscirev.2019.103003.

Varnes, D.J., 1978. Slope movement types and processes. In: Schuster, RL, Krizek, RJ (Eds.), Landslides, analysis and control, special report 176: Transportation research board. National Academy of Sciences, Washington, DC, pp. 12–33.

Viroulet, S., Baker, J.L., Rocha, F.M., Johnson, C.G., Kokelaar, B.P., Gray, J.M.N.T., 2018. The kinematics of bidisperse granular roll waves. J. Fluid Mech. 848, 836–875. https://doi.org/10.1017/jfm.2018.348.

Wang, G.H., Sassa, K., 2001. Factors affecting rainfall-induced flow slides in laboratory flume tests. Geotechnique 51 (7), 587–599. https://doi.org/10.1680/geot.2001.51.7.587.

Wang, G.H., Sassa, K., 2003. Pore-pressure generation and movement of rainfall-induced landslides: effects of grain size and fine-particle content. Eng. Geol. 69, 109–125. https://doi.org/10.1016/S0013-7952(02)00268-5.

Zanuttigh, B., Lamberti, A., 2007. Instability and surge development in debris flows. Rev. Geophys. 45 (3), RG3006. https://doi.org/10.1029/2005RG000175.

Zhang, J., Li, Y., Guo, X.J., Yang, T.Q., Liu, D.C., Yu, B., 2021. Temporal Characteristics of Debris Flow Surges. Front. Earth Sci. 9, 660655 https://doi.org/10.3389/feart.2021.660655.